THE ASTROPHYSICAL JOURNAL, 516:177–186, 1999 May 1

WHAT IS THE ACCRETION RATE IN NGC 4258?

CHARLES F. GAMMIE[1] AND RAMESH NARAYAN
Harvard-Smithsonian Center for Astrophysics, MS-51 60 Garden Street, Cambridge, MA 02138
AND
ROGER BLANDFORD
Theoretical Astrophysics, Caltech 130-33, Pasadena, CA 91125
Received 1998 June 26; accepted 1998 December 8

ABSTRACT

We estimate the accretion rate $\dot{M}$ onto the black hole in the nucleus of NGC 4258. The result is model dependent. We find that a thin disk that is flat out to $\gtrsim 2 \times 10^3 GM/c^2$ ($M \equiv$ black hole mass) and that has inclination equal to that of the masing disk must have $\dot{M} \simeq 0.01\ M_\odot\ \mathrm{yr}^{-1}$ for consistency with near-infrared data. A thin disk that is warped at $\sim 10^3 GM/c^2$ requires $\dot{M} \gtrsim 1.5 \times 10^{-4}\ M_\odot\ \mathrm{yr}^{-1}$ for consistency with near-infrared data. Reasonable warp models and the near-infrared data are not consistent with $\dot{M}$ as low as the $7 \times 10^{-5}\alpha\ M_\odot\ \mathrm{yr}^{-1}$ proposed by Neufeld & Maloney. An advection-dominated flow model combined with the X-ray data implies $\dot{M} \simeq 0.01\ M_\odot\ \mathrm{yr}^{-1}$. Consistency with a tight 22 GHz upper limit on the flux from the central source requires a transition radius of $\sim$(10–100)GM/c^2, although the 22 GHz upper limit may be relaxed by appeal to free-free absorption. Physical conditions in the observed VLBI jet features can also be related to conditions in the inner accretion flow. We conclude with a list of observations that might further constrain $\dot{M}$.

Subject headings: accretion, accretion disks — galaxies: individual (NGC 4258) — galaxies: nuclei — masers — X-rays: galaxies

1. INTRODUCTION

Most measurements of the physical properties of astronomical objects are fortunate if they obtain an accuracy of a factor of 2. In the rare instances when more precise measurements are possible, it is worth investing some effort to understand the object in detail and to uncover any additional possibilities for advancing astronomical knowledge. The orbiting maser spots in NGC 4258 offer one of these rare opportunities.

Water maser emission was first detected in the nucleus of NGC 4258 by Claussen, Heiligman, & Lo (1984). It was soon realized that the masers might lie in a disk (Claussen & Lo 1986). Nakai, Inoue, & Miyoshi (1993) discovered high-velocity maser emission, which Watson & Wallin (1994) interpreted as a natural outcome of maser emission from a disk. VLBI observations (Greenhill et al. 1995b; Miyoshi et al. 1995; Moran et al. 1995; Herrnstein, Greenhill, & Moran 1996) demonstrated that the maser spots are positioned on the sky as one would expect for a nearly edge-on thin disk. A model fit to the maser spots allows one to determine the central mass (Miyoshi et al. 1995). By measuring maser spot accelerations (Haschick & Baan 1990; Haschick, Baan, & Penn 1994; Greenhill et al. 1995c, 1995a; Herrnstein 1997) or proper motions (Herrnstein 1997) one can also directly determine a geometric distance.

The measurement of an accurate mass and distance eliminates two of the principal uncertainties in studies of active galactic nuclei (AGNs). The mass of the central object in NGC 4258 (which we will freely refer to as a black hole) is $(4.0 \pm 0.25) \times 10^7\ M_\odot$ (Herrnstein et al. 1998b; 1 σ). The distance is 7.3 ± 0.3 Mpc, with independent and consistent results from maser spot accelerations and maser spot proper motions (Herrnstein et al. 1997b).

[1] Also Isaac Newton Institute, 20 Clarkson Road, Cambridge CB3 0EH, UK.

Another important parameter of interest in AGN studies is the accretion rate $\dot{M}$. A number of estimates for $\dot{M}$ in NGC 4258 have appeared in the literature—Neufeld & Maloney (1995, hereafter NM): $7 \times 10^{-6}\alpha_{-1}\ M_\odot\ \mathrm{yr}^{-1}$, where $\alpha = 0.1\alpha_{-1} \lesssim 1$ is the usual dimensionless angular momentum diffusion coefficient of accretion disk theory (Shakura & Sunyaev 1973; Pringle 1981); Lasota et al. 1996: $0.014\alpha_{-1}\ M_\odot\ \mathrm{yr}^{-1}$; Cao & Jiang 1997: $8 \times 10^{-5}\alpha_{-1}\ M_\odot\ \mathrm{yr}^{-1}$; Maoz & McKee 1997: $7 \times 10^{-3}\ M_\odot\ \mathrm{yr}^{-1}$; Kumar 1997: $1.5 \times 10^{-3}\ M_\odot\ \mathrm{yr}^{-1}$. The purpose of this paper is to clarify some of the issues involved in obtaining an accurate estimate for $\dot{M}$ and to raise observational and theoretical questions, the answers to which might narrow the range of allowed rates.

This task is complicated by a number of factors. First, $\dot{M}$ may not be well defined because of variations in the mass flux over timescales of years to gigayears. Second, although the maser spots are superb probes of the orbital kinematics, and even dynamics, of the masing annulus, the nonlinear nature of maser emission complicates direct inferences about conditions in the bulk of the disk at that radius. Third, most of the accretion energy is released in the spatially unresolved region close to the black hole. Thus, the spectral energy distribution (inferred from infrared [IR], optical, and X-ray fluxes) constrains $\dot{M}$ only after being folded through a model for the inner accretion flow.

We begin in § 2 with a critical review of the data. The remainder of the paper is devoted to constraints provided by the masing disk (§ 3), the inner accretion flow (§ 4), and the jet (§ 5). A summary and discussion of observations that might further constrain $\dot{M}$ follows in § 6.

2. CRITICAL REVIEW OF DATA

2.1. *Masing Disk*

In addition to giving a mass and distance, maser observations also constrain the disk shape. Assuming the disk is thin and in centrifugal balance, the shape can be fully

described by the variation of the unit angular momentum vector with radius (see Appendix). The location of this unit vector is conveniently described in terms of its position angle $p(r)$ and inclination angle $i(r)$, where $i = 0$ corresponds to an orbiting ring of material whose angular momentum points directly at the observer.

The disk can be fitted with a flat model ($dp/dr = di/dr = 0$; Miyoshi et al. 1995), but a better fit to maser spot positions is obtained if $dp/d \ln r \sim 0.2$ rad (Herrnstein 1997). There may also be evidence for a flattening of the rotation curve consistent with $di/d \ln r$ of the same order but opposite sign (J. R. Herrnstein 1998, private communication).

2.2. *Nuclear Spectral Energy Distribution*

Chary & Becklin (1997) have recently reported *J*-, *H*-, and *K*-band (1.25, 1.65, 2.21 μm) observations of NGC 4258 in 0.″6 seeing. Using the *J*-band image as a baseline, they subtract a scaled *J*-band image from the *H* and *K* images and find a nuclear emission excess consistent with a point source. The excess is 1.1 mJy at *H* and 4.5 mJy at *K*. It is then possible to deduce the extinction and intrinsic luminosity of the source by assuming that the extinction has the same wavelength dependence as dust in the local interstellar medium and that the intrinsic spectrum has an approximately power-law form ($f_\nu \sim \nu^s$):

$$A_V = 20.1(1 + 0.21s) \text{ mag} , \quad (1)$$

$$\log [\nu L_\nu(H)/\text{ergs s}^{-1}] = 41.63 + 0.32s , \quad (2)$$

$$\log [\nu L_\nu(K)/\text{ergs s}^{-1}] = 41.51 + 0.19s . \quad (3)$$

The spectral index s might range from $\sim\frac{1}{3}$ for the classical thin disk spectrum to ~ -1, which is typical for an unobscured AGN. The implied flux at J is $0.2(2.62)^s$ mJy, which is small enough to justify the use of the *J*-band image as a baseline. Taking $R_V = 3.1$ (Spitzer 1978), the extinction implies an obscuring column

$$N_H = 3.8 \times 10^{22}(1 + 0.21s)(Z_\odot/Z) \text{ cm}^{-2} \quad (4)$$

($Z \equiv$ metallicity) or

$$\Sigma = 0.09(1 + 0.21s)(Z_\odot/Z) \text{ g cm}^{-2} . \quad (5)$$

These estimates are sensitive to the assumed extinction curve, since

$$\frac{d \ln \nu L_\nu(H)}{d \ln (A_H/A_K)} = -5.3 - 1.1s , \quad (6)$$

$$\frac{dA_V}{d \ln (A_H/A_K)} = -50 - 10s . \quad (7)$$

Evidently 10% variations in A_H/A_K can lead to factor-of-2 errors in the intrinsic luminosity. It is possible that the extincting dust has evolved to a larger characteristic size than in the local interstellar medium. The sense of the effect of grain size evolution, at least in the grain models of Laor & Draine (1993), is to decrease A_H/A_K and so increase the intrinsic luminosity.

Makishima et al. (1994) have reported *ASCA* observations of NGC 4258. They fitted a four-component model to the spectrum, including an obscured power law, an iron line, a Raymond-Smith plasma, and thermal bremsstrahlung. They find an integrated luminosity for the power-law component in the 2–10 keV band of $(4.4 \pm 1.1) \times 10^{40}$ ergs s^{-1} (at 7.3 Mpc) and an absorbing column $N_H = (1.5 \pm 0.2) \times 10^{23}(Z_\odot/Z)$ cm^{-2}, i.e., $\Sigma = 0.36$ g cm$^{-2}(Z_\odot/Z)$. The integrated luminosity implies $\nu L_\nu = 2.7 \times 10^{40}$ ergs s^{-1} at 4.5 keV, taking the mean of νL_ν across the 2–10 keV band.

The X-ray column is a factor of 4 larger than the column inferred from IR extinction. This may simply reflect uncertainties in the IR or X-ray absorption model. On the other hand, it raises the intriguing possibility that the absorbing column covers the X-ray source but only partially covers the more extended IR-emitting region.

The data of Makishima et al. are now publicly available through the *ASCA* data archives. We have tried fitting only an absorbed power law to the 2.5–10 keV data. While the total luminosity is robust, being mostly determined by the flux near 10 keV, our absorption column is lower than the Makishima et al. value. This suggests that the derived absorption column is sensitive to the presence of the thermal bremsstrahlung component in the Makishima et al. model and may be somewhat less reliable than the total luminosity. The detection of a narrow iron line reported by Makishima et al. (1994) also appears to be marginal.

Herrnstein et al. (1998a) report a 3 σ upper limit on the 22 GHz flux from the neighborhood of the compact object of 0.22 mJy, or $\nu L_\nu = 3.1 \times 10^{35}$ ergs s^{-1}. This is a strong upper limit, but it is possible that flux from the central source is depressed by free-free absorption. Since we can see the jets (§ 2.3), but not the central source, the absorption, if present, probably varies on a scale $L \lesssim 0.2$ pc. Assuming that the X-ray absorption arises in the same column, the 22 GHz free-free optical depth is

$$\tau_{\text{ff}}(22 \text{ GHz}) \simeq 5.7x^2\left(\frac{0.2 \text{ pc}}{L}\right)\left(\frac{T}{10^4 \text{ K}}\right)^{-3/2} , \quad (8)$$

where $x \equiv$ ionization fraction and we have ignored the logarithmic variation of the Gaunt factor away from 10^4 K. It thus seems plausible that there is significant free-free absorption of the central source.

Rieke & Lebosky (1978) report a detection in a 5″ aperture at 10 μm of 100 mJy, or $\nu L_\nu = 1.9 \times 10^{41}$ ergs s^{-1}. A consistent result at similar aperture size is reported by Cizdziel, Wynn-Williams, & Becklin (1985). Because of the large aperture we regard this as an upper limit rather than a detection.

Finally, the nucleus has been detected in polarized optical light by Wilkes et al. (1995). The polarized continuum has $f_\nu \sim \nu^{-1.1 \pm 0.2}$, with an amplitude $\nu L_\nu = 1.1 \times 10^{39}$ ergs s^{-1}. The polarized spectral lines have FWHM of order 2500 km s^{-1}, a velocity characteristic of radii just inside the masing disk. Because the composition and distribution of the scattering medium are poorly constrained, this measurement offers only the weak constraint $\nu L_\nu(5500 \text{ Å}) < 4 \times 10^{43}$ ergs s^{-1} (see Wilkes et al. 1995).

2.3. *Jet*

The jet in NGC 4258 is observed at milliarcsecond scales in the 22 GHz continuum with the VLBA (Herrnstein et al. 1997a) and at arcsecond and larger scales in radio, optical, and X-ray bands.

The VLBA jet was discovered by Herrnstein et al. (1997a), while higher signal-to-noise data have recently been presented by Herrnstein et al. (1998a). The northern jet has flux density $\simeq 3$ mJy, is variable on a timescale of weeks, and is unresolved. Its mean location is about 0.014 pc (= 17

light-days $=7500GM/c^2$) due north of the black hole, but its position varies significantly with time. The southern jet has flux density $\simeq 0.5$ mJy, has not varied significantly in flux or position, and is also unresolved. It is located about 0.035 pc ($=43$ light-days $=19{,}000GM/c^2$) due south of the black hole. The difference in brightness between the northern and southern jet is attributed by Herrnstein et al. (1997a) to free-free absorption in the masing disk. The blob locations are consistent with the jet being normal to the outer, masing disk. This suggests that the disk is not strongly warped, at least in position angle, between the masing disk and the radius where the jet is launched.

Radio and X-ray observations show a curious, twisted jet outflow both to the north and the south extending out to ~ 5 kpc (summarized by Cecil, Wilson, & Tully 1992; Cecil, Wilson, & DePree 1995b; Cecil, Morse, & Veilleux 1995a). The jet X-ray emission has a power $\sim 2 \times 10^{40}$ ergs s^{-1} and can be satisfactorily fitted by a thermal spectrum with temperature $T_X \sim 3 \times 10^6$ K. Associated with this jet are forbidden emission lines that appear to come from locally photoionized shocked plasma. The line widths suggest velocities of ~ 500 km s^{-1}.

3. MASING DISK

What can be directly inferred about the masing disk from the existence of the maser spots? Obviously they imply the existence of gas in a density and temperature regime appropriate to maser emission (see the discussion of Maoz & McKee 1997), but this does not tell us that the masing gas lies at the disk midplane. It is possible that the masing gas lies in a warm layer on whichever surface of the disk is exposed to the central source. Masing disk models that produce emission in X-ray–heated gas (Neufeld & Maloney 1995; Neufeld, Maloney, & Conger 1994) work equally well if that gas lies in a layer atop a colder disk.

Notice also that the existence of persistent maser spots does not necessarily imply that the masing gas is lumpy. Spots can be produced at velocity caustics (Wallin, Watson, & Wyld 1998), although if $\delta v \sim c_s$ then inevitably $\delta\rho \sim \rho$ as well. Even if the spots are due to density variations, they may well be transient waves. Compressive waves with $\lambda \sim H$ evolve on a timescale $\Omega^{-1} \simeq 1000$ yr, so the persistence of masing spots over shorter timescales does not imply that the masing spots are bound clumps.

An estimate for the density and temperature in the masing disk can be used to infer $\dot{M}$ using the usual steady state disk theory (Shakura & Sunyaev 1973):

$$\dot{M} = 3\pi\Sigma\alpha c_s^2/\Omega \, . \tag{9}$$

Here c_s (which may be interpreted as a thermal sound speed or a cloud velocity dispersion) is constrained by the small vertical dispersion in the maser spots to be $\lesssim 2.3$ km s^{-1} (Moran et al. 1995). NM estimate Σ by arguing that the disk makes a phase transition to an ionized state outside $\simeq 0.26$ pc, thereby explaining the outer edge of the masing disk.[2] Maoz & McKee (1997) require $n \sim 10^9$ cm^{-3} and $H \sim 10^{16}$ cm for consistency with their shock-produced maser model. Kumar (1997) develops a model of a clumped disk in which gravitational scattering of clumps of mass m_c off one another produces the anomalous viscosity. The cloud velocity dispersion $c_s \sim (Gm_c\Omega)^{1/3}$; Kumar then estimates the disk mass (and therefore Σ) to obtain $\dot{M}$.

Two significant assumptions go into equation (9). The first is that external torques such as MHD winds are negligible. An external torque per unit area T can drive steady accretion at a rate of $\dot{M} = -4\pi T/\Omega$ in a Keplerian disk. There is no good theory that connects T to the local temperature and surface density, so in principle external torques can drive accretion at an arbitrarily large rate. The only, very weak, constraint comes from measurements of the radial velocity of the systemic maser features.

The second assumption underlying equation (9) is that the disk is in a steady state. Even if $T \equiv 0$, the disk may have $\partial_r \dot{M}(r) \neq 0$. Possible reasons for this include the following: (1) the disk is subject to a thermal or viscous instability that makes accretion unstable, as in cataclysmic variables; (2) gas is, or has been, delivered to the nucleus with very small angular momentum so that it circularizes well inside the masing disk. If mass is steadily supplied from $r \gtrsim 0.26$ pc, one expects the disk to reach a steady state on the viscous timescale $t_v \equiv (\alpha\Omega)^{-1} \times (r/H)^2 \simeq 2.6 \times 10^9 \alpha_{-1}^{-1}(200 \text{ K}/T)(r/0.2 \text{ pc})^{1/2}$ yr.[3] This is a long time, and we know of no evidence that accretion has been steady in NGC 4258 over such a long timescale.

One place to look for such evidence is in the jet. If the jet is produced in the immediate vicinity of the black hole and the jet mass loss rate is closely coupled to the accretion rate, then it provides a fossil record of past accretion. The characteristic timescale for the jet is $t_J = R/V_J = 2.4 \times 10^6 (R/5 \text{ kpc})(2000 \text{ km s}^{-1}/V_J)$ yr, where V_J is the jet radial velocity. More detailed models of the jet suggest an age of at least 10^6–10^7 yr (e.g., van Albada & van der Hulst 1982; Martin et al. 1989). Thus, the jet provides a record over only a small fraction of the masing disk viscous timescale. The jet is roughly continuous over its length, however (there are no lengthy gaps in the jets; see for example Fig. 2 of Cecil et al. 1995b). This suggests approximately steady accretion over a time t_J. For standard α disk models for the inner accretion flow we find $t_v = t_J \sim 10^6$ yr at $r \sim 10^3 GM/c^2$ (the precise value depends on $\dot{M}$, α, etc.). Thus, only a small region of the accretion flow in NGC 4258 needs to be in a steady state.

4. INNER FLOW MODELS

Most of the accretion energy is extracted in the spatially unresolved region close to the black hole, at $r \sim 10^{13}$ cm (absent a strong wind at large radius, e.g., Blandford & Begelman 1998). Estimates for $\dot{M}$ in the inner flow must therefore be folded through a model, with significant attendant uncertainty. We consider a series of models for this region and use them to estimate $\dot{M}$ by comparison with observation.

Before going on, however, consider the following simple argument. We may write

$$\dot{M} = \frac{4\pi d^2}{\epsilon c^2} \int dv \, f_v \, b_v \, , \tag{10}$$

where $f_v \equiv$ observed flux and b_v is a beaming factor, $\ll 1$ if emission is beamed toward us, $\epsilon = 0.1\epsilon_{-1} \equiv$ accretion efficiency, and $d = 7.3$ Mpc. As a first approximation take $b_v = 1$ and let f_v be a power law that runs from 10 μm to 100

[2] Cao & Jiang (1997) similarly explain the radial extent of maser emission but incorrectly assume that external radiation is deposited at the midplane of an optically thick disk.

[3] Once the disk becomes optically thick, as it likely will in the masing disk or at slightly smaller radius, $T \sim (F/\sigma)^{1/4} \sim 200$ K, where $F \equiv$ the flux from central source.

keV and passes through the X-ray data and the extinction-corrected near-IR flux, $f_\nu \simeq 1.6(\nu/10^{15}\ \mathrm{Hz})^{-1.2}$ mJy. Then

$$\dot{M} = 1.7 \times 10^{-4} \epsilon_{-1}^{-1}\ M_\odot\ \mathrm{yr}^{-1}\ . \tag{11}$$

But b_ν can be very different from 1; for a flat, steady state disk at $i = 98°$ (or, equivalently, 82°), for example, $b_\nu(2\ \mu\mathrm{m}) \simeq 20$. A specific model is required for a more refined estimate of $\dot{M}$.

4.1. *Thin, Flat Disk Model*

Suppose that the central engine is just a thin, flat disk that radiates locally like a blackbody. On the $\nu^{1/3}$ portion of the classical thin disk spectrum,

$$f_\nu = 17.8 \dot{M}_{-4}^{2/3} |\cos(i)| \lambda^{-1/3}\ \mathrm{mJy}\ , \tag{12}$$

where λ is in microns and $\dot{M}_{-4}$ is the accretion rate in units of $10^{-4}\ M_\odot\ \mathrm{yr}^{-1}$. Inverting this equation,

$$\dot{M} \simeq 1.3 \times 10^{-6} f_\nu^{3/2} \lambda^{1/2} |\cos(i)|^{-3/2}\ M_\odot\ \mathrm{yr}^{-1}\ , \tag{13}$$

where f_ν is in mJy. Assuming that the IR data lie on the $f_\nu \sim \nu^{1/3}$ portion of the thin disk spectrum and that $i = 98°$, the IR data of Chary & Becklin require $\dot{M} = 0.011\ M_\odot\ \mathrm{yr}^{-1}$. Notice that the inclination correction is large because $\dot{M}$ depends nonlinearly on $\cos(i)$. Equation (13) also assumes the disk extends down to $r = 0$; if the disk is truncated properly (say at $r = 6GM/c^2$) then $\dot{M}$ must be evaluated numerically: $\dot{M} = 0.013\ M_\odot\ \mathrm{yr}^{-1}$.

Thin, flat disk spectra are shown in Figure 1 along with the data from § 2. The model spectra terminate at $\simeq 300\ \mu$m because parts of the disk are likely to be optically thin at longer wavelengths, causing gross departures from a blackbody. Four models are shown. The two solid lines show models at $i = 98°$ and $i = 45°$ with $\dot{M}$ adjusted to fit the IR data; for more nearly face-on disks $\dot{M}$ is reduced by an order of magnitude, although such an inclination seems unlikely since the large-scale jet, which is presumably normal to the inner disk, appears to be almost in the plane of the sky.

Some of the near-IR emission may be light from the central engine, reprocessed either in a disk or in a wind (e.g., Königl & Kartje 1994). Crudely speaking, the light must be reprocessed at $r \sim r_{1500} \sim 2.8 \times 10^3 L_{42}^{1/2}\ GM/c^2$, corresponding to a characteristic temperature of 1500 K for near-IR emission (dust grains much smaller than 1 μm can produce H- and K-band emission from a larger radius because they radiate inefficiently in the IR). Where is reprocessing important? Suppose $\mu(r, \phi)$ is the "obliquity" of the disk (the angle between the normal to the disk surface and the radius vector) and f is the fraction of intercepted radiation that is thermalized in the disk (so $1 - f$ is an effective albedo). Then reprocessing is dominant if $r \gtrsim (GM/c^2)(\epsilon f \cos\mu)^{-1}$. For a thin, flared disk $\cos\mu \sim H/R \ll 1$, so that, in a standard α disk model over a large range of $\dot{M}$, reprocessing is not dominant at $r \sim r_{1500}$.

The two dashed lines in Figure 1 show flat, thin disks with NM's $\dot{M}$. The lower flux model uses NM's $\dot{M}$ while conservatively setting $\alpha = 0.1$, terminating the disk at $6GM/c^2$, so the efficiency is $\simeq 0.06$, and setting the inclination of the inner disk to that of the outer disk. The higher flux model sets all parameters to produce the maximum possible flux from the NM model. It sets $\alpha = 1$ (this seems very unlikely to us for all proposed angular momentum

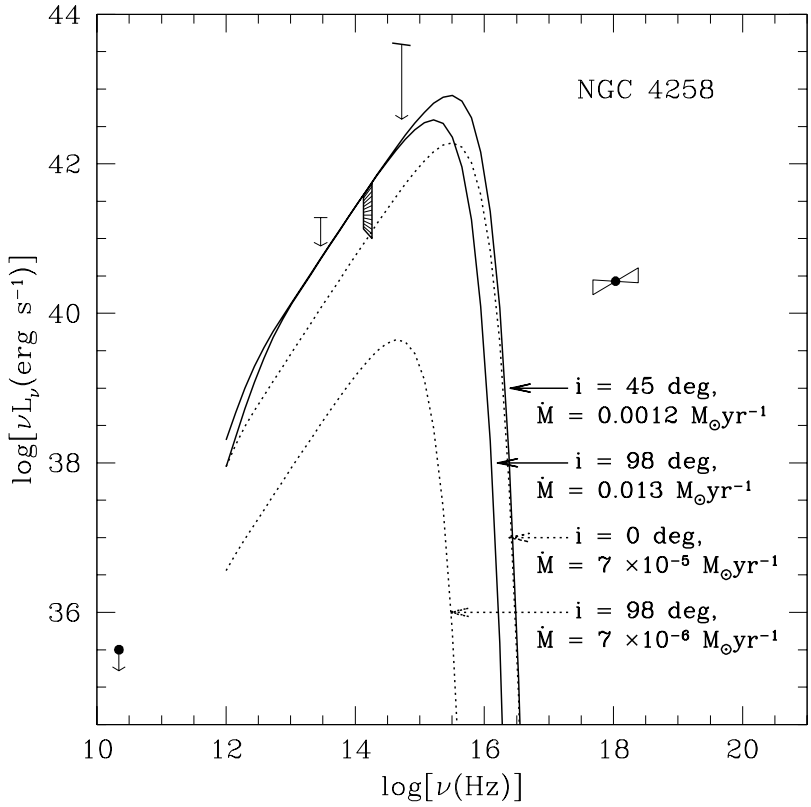

FIG. 1.—Observed spectrum compared with steady state thin, flat disk models. The gear-shaped symbol near 10^{14} Hz summarizes the IR data of Chary & Becklin (1997); since their inferred luminosity depends on spectral slope, a successful model must transit the "gear" at the slope indicated by the thin lines joining the two dark vertical lines at the H and K bands. The solid lines are models with $i = (45°, 98°)$ and $\dot{M} = (0.0012, 0.013)\ M_\odot\ \mathrm{yr}^{-1}$; the dashed lines have $i = (98°, 0°)$ and $\dot{M} = (7 \times 10^{-6}, 7 \times 10^{-5})\ M_\odot\ \mathrm{yr}^{-1}$, corresponding to Neufeld & Maloney's (1995) accretion rates for $\alpha = (0.1, 1)$.

transport mechanisms except gravitational instability, which is in any case not present in the NM model at this $\dot{M}$), it sets the inclination to 0 (unlikely because of the orientation of the large-scale jet), and truncates the disk at GM/c^2 (the turnover in the spectrum at $10^{15.5}$ Hz is in error by order unity because we have not used relativistic photon transport). The change in inclination increases the near-IR flux by $\simeq 7$, the change in α increases the near-IR flux by $\simeq 5$, and the energy available from the increased efficiency is mostly expended in the UV. The model still lies a factor of $\simeq 5$ below the near-IR data.

4.2. *Thin, Warped Disk Model*

If the disk is warped then disk obliquity can be larger and reprocessing can dominate internal heating at those radii that produce the near-IR flux. As an illustration we have constructed a "naive" warped disk in which light intercepted by the disk is reradiated as a blackbody. The disk extends from $r = GM/c^2$ to 0.26 pc and has constant $\dot{M}$. A central source of luminosity $0.42\dot{M}c^2$ is used to calculate the reprocessing (this may overestimate the flux intercepted by the disk because it neglects the apparent inclination of the inner disk as seen from the outer disk). In the Appendix we describe the shape of our model warp, which is chosen to be consistent with masing disk observations and to produce an inner disk oriented approximately normal to the large-scale jet. The Appendix also explains how to calculate the spectral energy distribution of a thin, warped disk.

Figure 2 shows the resulting spectrum. We have chosen $\dot{M} = 7 \times 10^{-5}\ M_\odot\ \mathrm{yr}^{-1}$, the maximal ($\alpha = 1$) NM value. Since we have pushed all the model parameters so as to maximize the flux, the resulting spectrum is an upper envelope for models consistent with the NM $\dot{M}$ (the warp shape is nonunique, but we have intentionally included a generous warp at the reprocessing radius; see the Appendix); an $\dot{M}$ of at least $1.5 \times 10^{-4}\ M_\odot\ \mathrm{yr}^{-1}$ is required for consistency with the near-IR data. Lowering α, using an evolved grain population to estimate the IR extinction correction, lowering the efficiency (i.e., lowering the spin of the black hole), including the apparent inclination of the inner disk as seen from the outer disk in reprocessing calculations, and reducing the amplitude of the warp would all reduce the flux. It thus seems unlikely to us that $\dot{M}$ is as low as proposed in the NM model, at least as presented by Neufeld & Maloney (1995). It may be that a more refined treatment of the masing layer would relocate their phase transition radius to make it consistent with a higher $\dot{M}$. It is also possible that the entire disk is not in a steady state and thus the accretion rates at the masing disk and at the inner disk are different (see § 3).

It is remarkable that this $\dot{M} = 7 \times 10^{-5}\ M_\odot\ \mathrm{yr}^{-1}$ model can come within a factor of a few of matching the IR data, which are also fitted by an $\dot{M} \simeq 0.01\ M_\odot\ \mathrm{yr}^{-1}$ flat disk model. Four factors contribute to this effect: (1) reprocessing enhances the 2 μm flux; (2) reprocessing makes the spectrum shallower at 2 μm thus reducing the extinction correction; (3) the inclination of the warped disk varies so that the reprocessing portion of the disk (at $\sim 1300GM/c^2$) is more nearly face-on; (4) the assumed efficiency is larger in the warped disk model.

Our warped disk model is naive in the sense that the reprocessed emission is assumed to be a blackbody. Dust

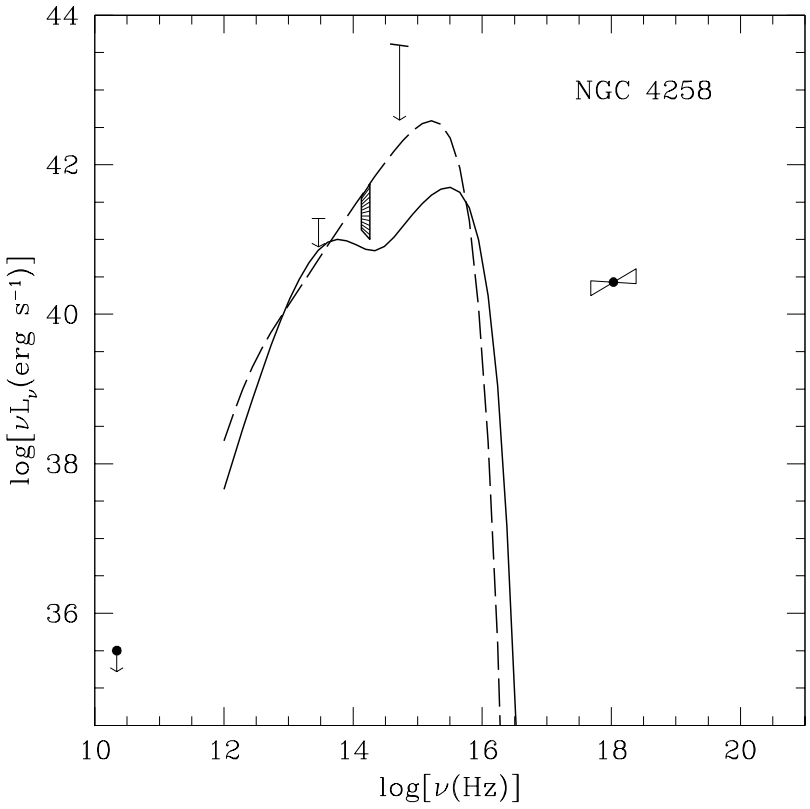

FIG. 2.—Observed spectrum compared with steady state thin, warped disk models. The data are as in Fig. 1. The solid line is the warped disk model, which has $\dot{M} = 7 \times 10^{-5}\ M_\odot\ \mathrm{yr}^{-1}$; this is the maximal ($\alpha = 1$) Neufeld & Maloney (1995) accretion rate. The model is truncated at $r = GM/c^2$, i.e., the black hole has maximum prograde rotation. For comparison, the dashed line shows the thin, flat disk model with $i = 98°$ accreting at $\dot{M} = 0.013\ M_\odot\ \mathrm{yr}^{-1}$.

grains in the disk atmosphere can intercept much of the incoming radiation and reradiate part of it as a dilute blackbody with T greater than the disk effective temperature. This effect has been considered in the context of quasar disks by Sanders et al. (1989) and Phinney (1989) and in the context of circumstellar disks by Chiang & Goldreich (1997).

A reprocessing model for the H- and K-band flux can be tested via long-term monitoring. If the light is reprocessed, then IR variability should be correlated with X-ray variability, with delays on order the light travel time $r_{1500}/c \simeq 5.5 \times 10^5 L_{42}^{1/2}$ s.

New mid-IR data at higher spatial resolution would also provide a test of the reprocessing model. Flat disk and warped disk models differ substantially at these wavelengths. If the Rieke & Lebosky (1978) upper limit were to turn into a detection then flat disk models would require an $\dot{M} \simeq 0.1\ M_\odot\ \mathrm{yr}^{-1}$ and would be inconsistent with the near-IR data. A mid-IR detection would also constrain the universe of warp shapes in warped reprocessing disk models.

Finally, while we have not explicitly fitted the X-ray emission using a thin disk plus corona model (e.g., Haardt & Maraschi 1991), it is generally acknowledged that it is possible to do so, since there are a number of free parameters associated with the corona.

4.3. *Advection-dominated Flow Model*

An alternative to the thin disk plus corona model for the inner accretion flow is the two-temperature advection-dominated accretion flow (ADAF) model (Ichimaru 1977; Narayan & Yi 1994; Narayan & Yi 1995b; Abramowicz 1995; see Narayan 1997; Narayan et al. 1998a for reviews). ADAFs are optically thin and geometrically thick, with $H/R \sim 1$. They have been used to successfully fit the spectral energy distribution of accretion flows onto both stellar mass and supermassive black holes. In their simplest form, ADAFs approximate the flow as nonradiative, with nested spherical surfaces moving radially inward with an angular velocity given by the value on the equatorial plane. Radial pressure gradients combine with centrifugal force to oppose gravity, and radial motion is fast, although subsonic until it approaches the event horizon. There is hypothesized to be a large viscous stress ($\sim \alpha P$, where P is the pressure) that transports angular momentum radially outward.

The ADAF approach has some dynamical shortcomings. First, it does not take account of angular velocity gradients on spherical surfaces. This appears to be a reasonable approximation far from the black hole in the self-similar region of the flow (cf. Narayan & Yi 1995a), but the approximation may break down close to the hole, especially close to the symmetry axis. This is relevant for understanding whether the flow forms a funnel and a jet. The indications are that there is no funnel when $\alpha \gtrsim 0.01$ (Narayan, Kato & Honma 1997; Chen, Abramowicz, & Lasota 1997; Abramowicz et al. 1996; Gammie & Popham 1998; Popham & Gammie 1998), although this conclusion is not certain. Second, the solutions assume vertical hydrostatic equilibrium, which is suspect in the supersonic region close to the hole. This approximation should not have a direct impact on the emergent radiation, however. Finally, in these solutions, the gas has a positive Bernoulli constant and always has enough energy to escape the hole (see Narayan & Yi 1994, 1995a; Narayan et al. 1997). This arises because of the inevitable, outward radial transport of energy by the viscous stress, which is balanced exactly by inward advective energy transport. This balance must be maintained everywhere. If it is not, then it is possible that energy may be carried away by a wind (see Blandford 1998; Blandford & Begelman 1998).

Counterbalancing these shortcomings is the fact that the ADAF is the only model of hot accretion flows that attempts to calculate the dynamics, thermal structure, and radiative spectrum of the gas self-consistently. Other approaches, e.g., coronal models, leave most details of the dynamics unspecified and allow far greater freedom in choosing the properties of the radiating plasma.

Lasota et al. (1996) proposed a model for NGC 4258 made up of a thin disk extending outward from the transition radius $r_{\rm tr}$ and an ADAF extending inward to the black hole. The mass accretion rate in the model is essentially fixed by the X-ray data point to be of order $0.014\alpha_{-1}$ $M_\odot\ \mathrm{yr}^{-1}$; Lasota et al. take $\alpha_{-1} = 1$. One free parameter remains: $r_{\rm tr}$. At the time Lasota et al. (1996) was written the data did not constrain $r_{\rm tr}$. Two results have since appeared that do: the 22 GHz upper limit of Herrnstein et al. (1998a) and the IR detections of Chary & Becklin (1997). There has also been considerable improvement in the calculation of the ADAF model spectral energy distribution. Relativistic effects (Gammie & Popham 1998 and references therein) and advective heating of the electrons (Nakamura et al. 1997) are now included; details of the computation are described by Narayan et al. (1998b), who apply the ADAF model to the Galactic center source Sgr A*.

Figure 3 shows the spectral energy distribution of NGC 4258 corresponding to three ADAF models, with $r_{\rm tr} = (10, 10^{1.5}, 10^2) \times 2GM/c^2$ and $\dot{M} = (0.012, 0.008, 0.006)\ M_\odot\ \mathrm{yr}^{-1}$, which we call models 1, 1.5, and 2. The disk outside $r_{\rm tr}$ is thin and flat and radiates like a blackbody. All models use standard values for other parameters: $\alpha = 0.3$, $\beta = 0.5$, and $\delta = 10^{-3}$ ($\beta \equiv p_{\rm gas}/p_{\rm tot}$, $\delta \equiv$ fraction of dissipation going into electrons). Model 1 (2) has the most (least) flux in the optical (radio). Evidently model 1 fits the IR data best and does not violate the 22 GHz upper limit, although model 1.5 also gives an acceptable fit to the IR data and may have better agreement with the spectral index of the scattered optical light. Model 2 is close to violating the 22 GHz upper limit.

The ADAF model predicts the flux from the central accretion flow at several wavelengths that may be observed in the near future. At 10 μm the observed flux should not be below the thin disk value (see eq. [12]) of (200, 150, 130) cos (i) mJy for models (1, 1.5, 2); it can be larger because of reradiation by dust. At 22 GHz the flux should be (0.017, 0.082, 0.23) mJy with $s \equiv d\ln f_\nu/d\ln \nu \approx 1.5$ for all three models. Higher frequency interferometry may be possible; at 100 GHz, $f_\nu = (0.13, 0.65, 1.5)$ mJy, with $s = (1.8, 1.4, 1.3)$, and at 690 GHz, $f_\nu = (3.4, 10.0, 18.0)$ mJy, $s = (1.6, 1.3, 1.0)$. At 5500 Å the expected flux is (38, 8.4, 0.59) mJy with $s = (-0.39, -2.0, -2.2)$; recall that Wilkes et al. (1995) find $s = -1.1$. The model is adjusted so that the flux at 10 keV fits the observations; at 10 keV the predicted photon index is (1.9, 1.9, 2.0), which may be compared with the observed index of 1.78 ± 0.29. Finally, the expected flux at 30 keV is $(3.1, 3.4, 3.4) \times 10^{-6}$ photons cm^{-2} s^{-1} keV^{-1}, and the photon index for all three models is 2.0. For comparison we have also calculated a similar series of models with $\alpha = 0.1$. These are shown as dashed lines in Figure 3.

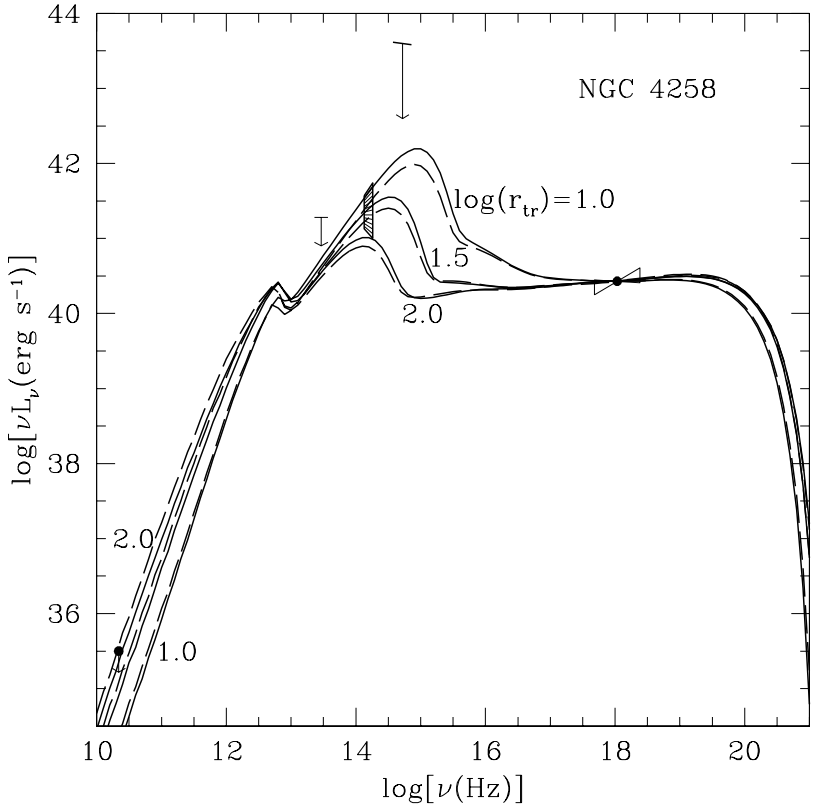

FIG. 3.—*Solid lines*: series of ADAF models with varying transition radii r_{tr} and $\alpha = 0.3$. The $\dot{M}$ vary so as to match the X-ray data. The models have $r_{tr} = (10, 10^{1.5}, 10^2)2GM/c^2$ and $\dot{M} = (0.012, 0.008, 0.006)\ M_\odot\ \mathrm{yr}^{-1}$. The optical/IR flux increases as the transition radius is reduced. *Dashed lines*: same as solid lines except $\alpha = 0.1$ and $\dot{M} = (0.073, 0.056, 0.045)\ M_\odot\ \mathrm{yr}^{-1}$.

4.4. *Ion Torus Model*

A related, although distinct, alternative to the ADAF is the ion torus (Rees et al. 1982). As in the ADAF, it is assumed that the plasma is two temperature with most of the pressure being supplied by the ions (see Shapiro, Lightman, & Eardley 1976 for the first application of the two-temperature idea to accretion) and that the radiative losses are small. The viscosity is assumed to be small enough (low α), however, that poloidal motion can be ignored in the equation of hydrostatic equilibrium. In its simplest manifestation, the specific angular momentum is constant and the surface of the torus is a surface of constant binding energy. As the radiative losses are small, the binding energy is quite low (relative to c^2 per unit mass) and plasma flows onto the black hole through an equatorial cusp with this energy and consistent with having lost little of its binding energy. This approach can accommodate the peculiar relativistic features of the Kerr metric (Abramowicz, Jaroszyński, & Sikora 1978).

Following previous work on thick disks, the ion torus model simply specifies the angular momentum profile rather than solving an angular momentum equation, and this is a serious weakness. Also, the model has no ready prescription for describing the gas inflow and, consequently, the thermal structure. In addition, tori of this sort are subject to hydrodynamical instability (Papaloizou & Pringle 1984), which calls into question the assumption of slow angular momentum transport.

Nonetheless, ion tori do have one feature that is important in the present context: they naturally create a pair of funnels in which magnetic flux can be concentrated so as to extract energy from the central spinning black hole and to power the jets. According to the work of Narayan et al. (1997), Chen et al. (1997), Abramowicz et al. (1996), and Popham & Gammie (1998), funnels are likely to be most prominent in low-α flows (ion tori) and are much less pronounced in high-α flows (standard ADAFs).

4.5. *General Constraints*

The failure to detect radio emission from the location of the black hole has some more general implications. Although we have demonstrated that ADAF models can be made to be consistent with this upper limit, alternative models that admit a nonthermal distribution of relativistic electrons to be accelerated directly are quite tightly constrained.

Let us suppose that there is a radio photosphere where the optical depth to synchrotron self-absorption becomes unity. Let it be located at a radial distance $r_p = 10^{14} r_{p14}$ cm from the black hole. The 22 GHz upper bound on the flux implies that the radio brightness temperature of this photosphere must satisfy

$$T < 2 \times 10^{11} r_{p14}^{-2}\ \mathrm{K} \tag{14}$$

(Herrnstein et al. 1997a). The corresponding energy of the electrons emitting at 22 GHz is $\sim 3kT \sim E_p \sim 70 B_p^{-1/2}$ MeV. These electrons radiate at $\sim \gamma^2 B$ MHz (cf. Rybicki & Lightman 1979), and so we conclude that the magnetic field strength at the photosphere satisfies $B_p = B(r_p) \gtrsim r_{p14}^4$ G (assuming that it is significantly less than the cyclotron field, ~ 7000 G). In other words the magnetic pressure must satisfy $P_{\mathrm{mp}} \gtrsim 0.04 r_{p14}^8$ dynes cm^{-2}. We use the theory of

synchrotron radiation to solve for the radius of the 22 GHz photosphere:

$$r_{p14} \sim 10 f_e P_{\rm mp}^2 , \tag{15}$$

where f_e is the ratio of the emitting electrons to the magnetic pressure. Now, in order not to exceed the radio flux upper limit, we require that $r_{p14} \lesssim 1.3 f_e^{0.07} \sim 20(GM/c^2) f_e^{0.07}$ and, equivalently, $P_{\rm mp} \lesssim 1.1 f_e^{-0.03}$ dynes cm^{-2}. As emphasized below, however, typical pressures in accretion flows are generally expected to exceed ~ 1 dynes cm^{-2} by a large factor, so this is a fairly stringent constraint.

ADAF models satisfy this constraint because they ignore extraneous relativistic particle acceleration so that the electron distribution function is thermal and exponentially declining at energies below E_p. (Mahadevan & Quataert 1997 have shown that the thermalization timescale for the electrons in an ADAF is shorter than the flow timescale, so that the assumption of a thermal particle distribution is consistent.) What we see from the analysis in this section is that this assumption is necessary.

Disk corona models generally do postulate relativistic particle acceleration. The accelerated particles might be expected to cause observable radio emission, and so the limit on the 22 GHz brightness temperature is a serious constraint.

There are some processes that can suppress radio synchrotron emission. The Razin effect is important at densities above $\sim 10^9 B_p$ cm^{-3}. Second, relativistic Coulomb interactions and synchrotron loss may cool freshly accelerated electrons to keep their steady pressure at a low level. This happens on timescales competitive with the inflow timescale. Finally, as discussed in § 2, free-free absorption may extinguish the radio source.

5. JET

It is clearly of interest to relate the observed VLBI jets to the gas flow close to the black hole. If we consider the northern VLBI component, we find that, at a projected distance of $r_\perp \sim 4 \times 10^{16}$ cm, the 22 GHz flux density is ~ 3 mJy. If we suppose that the unresolved source is the base of a jet with an opening angle of $\sim 10^\circ$ (cf. Herrnstein et al. 1997a) propagating nearly perpendicular to the line of sight with a bulk Lorentz factor Γ, then the radio brightness temperature is only $\sim 2 \times 10^9$ K. Even allowing for relativistic beaming this is too low for synchrotron self-absorption to be important, and it seems reasonable to assume that both radio components are optically thin at this frequency. Let us now assume that the relativistic energy density in the jet is not much smaller than the magnetic energy density. A straightforward calculation relates the minimum power carried by the relativistic electrons (and, quite possibly, positrons) in the jet to Γ and to the ratio β_e of the electron energy density to the magnetic energy density (assumed >1):

$$L_{\rm jet} \sim 7 \times 10^{42} \beta_e^{0.4} \left(\frac{\Gamma}{10}\right)^{3.4} \ {\rm ergs}^{-1} \tag{16}$$

(see, e.g., Blandford 1990). The strong dependence of the minimum jet power on the Lorentz factor is due to a combination of the bulk energy and the diminution of the observed flux by relativistic beaming when the observer is located roughly perpendicular to the jet direction. We see that if jets have ultrarelativistic flow speeds, then they probably carry off significantly more power than is radiated directly.

The power in the jet may be extracted directly from the spin of the black hole (Blandford & Znajek 1977). If, instead, the power is derived from the accretion flow, then the jet implies a certain minimum mass accretion rate

$$\dot{M} \sim 1.2 \times 10^{-3} \epsilon_{-1}^{-1} \beta_e^{0.4} \left(\frac{\Gamma}{10}\right)^{3.4} M_\odot \ {\rm yr}^{-1} . \tag{17}$$

Notice that this is similar to the estimates of $\dot{M}$ obtained earlier by fitting the observed IR spectrum.

The pressure in the jet $\sim 0.07 \beta_e^{0.4} (\Gamma/10)^{1.4} (r/4 \times 10^{16}$ cm$)^{-2}$ dynes cm^{-2} must be confined transversely. If we evaluate this at the transition radius of the ADAF solution, then the jet pressure is $\sim 700 (\Gamma/10)^{1.4} \beta_e^{0.4}$ dynes cm^{-2}. For comparison, the pressure in the ADAF flow is

$$P \sim \frac{8000}{\alpha_{-1}} \left(\frac{\dot{M}}{10^{-2} M_\odot \ {\rm yr}^{-1}}\right) \left(\frac{r_{\rm tr}}{60 GM/c^2}\right)^{-5/2} {\rm dynes \ cm}^{-2} . \tag{18}$$

We note that, although the formation of funnels appears to be problematic in ADAFs with $\alpha \gtrsim 0.01$ (Narayan et al. 1997; Gammie & Popham 1998; Chen et al. 1997; Abramowicz et al. 1996), the pressure required to confine a jet able to account for the observed radio sources is probably present. An ion torus, by contrast, can naturally exert more pressure than a high-α ADAF as long as it is unable to cool. If $\dot{M} \lesssim 10^{-4} M_\odot$ yr^{-1}, however, it does not seem possible to supply enough pressure to confine a relativistic jet.

6. DISCUSSION

To sum up, we have used a series of models to estimate the accretion rate onto the black hole in NGC 4258. A thin, flat disk model with inclination equal to that of the masing disk gives $\dot{M} \simeq 10^{-2} M_\odot$ yr^{-1}; the key constraint here is the near-IR data of Chary & Becklin (1997). This model permits $\dot{M}$ as low as $\approx 10^{-3} M_\odot$ yr^{-1}, but only if the inner disk is nearly face-on and flat out to $\gtrsim 2 \times 10^3 GM/c^2$ (so that reprocessing is unimportant in the near IR) and then the disk warps at a larger radius so as to match the orientation of the masing disk. A nearly face-on disk such as this seems implausible given the orientation of the large-scale jet.

A thin, warped disk model is consistent with $\dot{M} \gtrsim 1.5 \times 10^{-4} M_\odot$ yr^{-1}. Near this lower limit the disk must be strongly warped at $\sim 1500 GM/c^2$ so that a large fraction of light from the central source is reprocessed into the near IR. We consider a warped disk model with $\dot{M} = 7 \times 10^{-5} \alpha$ and $\alpha = 1$, the maximum accretion rate consistent with the model of the masing disk proposed by Neufeld & Maloney (1995). If we push all model parameters so as to maximize the near-IR flux, the model is still not consistent with the observations. While this may reflect a problem with the assumptions underlying the NM model, it is also possible that the accretion rate in the masing disk is different from that in the inner flow, either because of an instability in the disk or because the flow is fed directly at a radius within the masing disk.

An ADAF model has $\dot{M}$ fixed by the X-ray flux to be $\simeq 10^{-2} M_\odot$ yr^{-1}. If the ADAF turns into a thin, flat disk outside a transition radius $r_{\rm tr} = (10$–$100) GM/c^2$, then it is naturally consistent with the near-IR data and the 22 GHz

upper limit of Herrnstein et al. (1998a). The Herrnstein et al. upper limit also constrains corona models. If the observed X-ray emission in NGC 4258 is from a corona, then the corona must be primarily thermal rather than nonthermal, since otherwise it would produce more radio flux than observed. This limits the kinds of relativistic acceleration one can invoke in the corona. The 22 GHz upper limit may be weakened, however, if there is significant free-free absorption at this frequency, which we argue in § 2.2 is plausible.

The minimum power in the jet in NGC 4258 also constrains $\dot{M}$, provided the jet power is derived from the accretion flow and not from the spin of the black hole. The resulting estimate for $\dot{M}$ (cf. eq. [17]) is similar to that obtained by fitting the IR spectrum. We have not considered models with disk winds; these can have large $\dot{M}$ at the masing disk even if the surface density and temperature are low. The wind can also produce additional reprocessed radiation.

Several observational tests would help to constrain the nature of the accretion flow in NGC 4258 and hence $\dot{M}$:

Iron line.—Detection of a relativistically broadened iron Kα line would rule out a standard ADAF model for NGC 4258, as it would imply cold material close to the event horizon.

Near-infrared photometry.—Much of our discussion relies on the near-infrared data of Chary & Becklin (1997). It is important to confirm the flux and nonstellar pointlike nature of the emission.

Midinfrared photometry.—A midinfrared detection would constrain the flow model at those radii inside the masing disk where 10 μm emission is produced. The thin, flat disk model, for example, predicts a 10 μm flux of ≈ 20 mJy, a factor of ≈ 5 below the upper limit of Rieke & Lebosky (1978). Also, detection of dust features in emission, coupled with a more sophisticated reprocessing model, would constrain the warp and physical conditions in the reprocessing gas.

Infrared variability.—Reprocessing models for the near-IR emission predicts that near-IR variability should be correlated with X-ray variability, with a minimum timescale of order $t_r = r_{1500}/c \simeq 5.5 \times 10^5 L_{42}^{1/2}$ s or about a week. A flat disk model predicts that the emission should be steady over much longer timescales; a nonthermal model would produce shorter timescale variability.

Multifrequency VLBI.—VLBI observations at lower frequencies than 22 GHz may tighten the general constraints on relativistic particle acceleration close to the black hole (see § 4.5), absent free-free absorption of the central source. Higher frequency VLBI may be able to test the importance of free-free absorption. If the absorption is weak at 22 GHz, then the central source might be detected at higher frequency; ADAF models predict $f_\nu \sim \nu^{1.5}$ near 22 GHz.

X-ray absorption variability.—If the X-ray–absorbing column is located near the masing disk, rather than being a dense foreground cloud, then the timescale for variation in the absorption should be of order $t_{\rm var} = L/v_\phi$, where L is the characteristic scale of the absorber and v_ϕ is the local circular velocity. If the absorber is located in the disk, for example, then $t_{\rm var} \simeq 6(r/0.3\ {\rm pc})^2(T/10^4\ {\rm K})^{1/2}$ yr.

This work was supported in part by NSF grants AST 94-23209 and AST 95-29170 and NASA grants NAG 5-2837 and NAG5-7007. We thank A. Esin for assistance with the *ASCA* data, and R. Chary, L. Greenhill, J. Herrnstein, J.-P. Lasota, and the referee for helpful comments.

APPENDIX A

SPECTRUM OF A WARPED DISK

We consider a warped disk model composed of centrifugally supported rings. Each ring has orbital angular momentum along the unit vector $\boldsymbol{l}(r) = [\cos(p)\sin(i), \sin(p)\sin(i), \cos(i)]$; $\hat{\boldsymbol{x}} = (1,0,0)$ points north in the plane of the sky and $\hat{\boldsymbol{z}} = (0,0,1)$ points toward us. We largely follow the notation of Pringle (1996), except that we substitute position angle $p(r)$ and inclination angle $i(r)$ for Pringle's γ and β, respectively.

One can erect a nonorthogonal coordinate system (r, ϕ) on the surface of the disk by taking $\phi = 0$ where the disk descends through the plane of the sky. The vector

$$\boldsymbol{dA} = r\,dr\,d\phi\left\{\boldsymbol{l} - \hat{\boldsymbol{r}}\left[\cos(\phi)\sin i\,\frac{dp}{d\ln r} - \sin\phi\,\frac{di}{d\ln r}\right]\right\} \tag{A1}$$

is the differential area element (normal to the surface of the disk); here $\hat{\boldsymbol{r}} = (\cos\phi\sin p + \sin\phi\cos p\cos i, \sin\phi\sin p\cos i - \cos\phi\cos p, -\sin\phi\sin i)$ is the radial unit vector pointing at the location (r, ϕ) on the disk. These results are derived by Pringle (1996). We shall also refer to the unit normal $\boldsymbol{n} \equiv \boldsymbol{dA}/|\boldsymbol{dA}|$.

Then

$$\nu L_\nu = 4\pi\nu \int \boldsymbol{dA}\cdot\hat{\boldsymbol{z}} I_\nu(r, \phi, \boldsymbol{n}, \hat{\boldsymbol{z}}) V(r, \phi)\ . \tag{A2}$$

Here I_ν is the intensity at the disk, which may be a function of the direction $(\boldsymbol{n}, \hat{\boldsymbol{z}})$ at which the line of sight pierces the disk and V is a "visibility" function that is 0 if the point (r, ϕ) is obscured by another piece of the disk and 1 otherwise. One way of calculating V is to search for zeros of $\boldsymbol{o}\cdot\boldsymbol{l}(|\boldsymbol{o}|)$, where $\boldsymbol{o}(z) = r\hat{\boldsymbol{r}} + z\hat{\boldsymbol{z}}$, $z > 0$ traces out the line of sight from (r, ϕ) to the observer.

To estimate I_ν we assume the disk radiates like a blackbody at temperature T_e, $I_\nu = B_\nu(T_e)$. We fix T_e via

$$\sigma T_e^4 = \frac{3}{8\pi}\Omega^2\dot{M} + \frac{L}{4\pi r^2}(\hat{\boldsymbol{r}}\cdot\boldsymbol{n})V'(r, \phi)S(\boldsymbol{n}, \hat{\boldsymbol{z}}, \hat{\boldsymbol{r}})\ . \tag{A3}$$

The first term accounts for internal dissipation (external torques vanish, and the disk is in a steady state), and the second for reprocessed radiation. We set $L = 0.42\dot{M}c^2$, corresponding to a Kerr black hole in maximum prograde rotation. V' is another visibility function that is 1 if an observer at (r, ϕ) can see the central source and 0 otherwise. S is 1 if we are looking at the face of the disk that is exposed to the central source [mathematically, $(\boldsymbol{n} \cdot \hat{\boldsymbol{r}})(\boldsymbol{n} \cdot \hat{\boldsymbol{z}}) < 0$] and 0 otherwise; this term is included because very little (of order $1/\tau$, where τ is the Rosseland mean optical depth) of the reprocessed flux exits through the unexposed face.

Finally, we must choose $i(r)$, $p(r)$. The theory of warps is not yet sufficiently developed to offer any guidance here. While Pringle (1996) has discovered a radiation-driven warping instability that might account for the warp, the condition for instability given in Pringle's equation (4.3), together with the relation $v_2/v_1 \approx (2\alpha^2)^{-1}$ (Papaloizou & Pringle 1983) implies that NGC 4258's disk is not unstable at $r \simeq 10^3 GM/c^2$ unless $\alpha > 0.7$ and is not unstable at the masing disk unless $\alpha > 0.2$. We must therefore extract the warp shape from observational evidence using some reasonable assumptions.

The inclination obtained by fitting a flat disk, or a disk warped only in position angle, to the maser spots is 98° (Miyoshi et al. 1995; the angular momentum vector of the disk actually points slightly *away* from us). Likewise, $p \simeq 180°$ at the masing disk. Fits indicate that $dp/d\ln r \simeq 0.2$ rad and that $di/d\ln r \simeq 0$ to -0.2 rad (Herrnstein 1997). The large-scale radio jet runs very nearly north-south, so we want the inner edge of the disk to have $p(r = r_{\rm in} = GM/c^2) \simeq 180°$. We are not allowed to let the disk cover the line of sight inside 0.26 pc, since that would probably produce too much absorption. We also assume that the disk warps smoothly and is normal to the jet at $r = r_{\rm in}$; the true situation could be more complicated if the Bardeen-Petterson effect (Bardeen & Petterson 1975) forces the inner disk to warp sharply to bring it into alignment with the spin of the black hole. A simple curve that satisfies all these constraints is

$$i = 1.83 + 0.022 \ln (r/r_{\rm in}) \cos A \text{ rad} , \tag{A4}$$

$$p = 3.23 - 0.022 \ln (r/r_{\rm in}) \sin A \text{ rad} , \tag{A5}$$

where $A = 0.91 \ln (r/r_{\rm in})$; this forms a loose logarithmic spiral on the unit sphere around $i = 105°$ and $p = 185°$. This warp has $|di/d\ln r| \sim |dp/d\ln r| \sim 0.1$ rad around $1500GM/c^2$, which is the region that produces reprocessed near-IR emission.

The reprocessing model could be improved by using a nonblackbody disk atmosphere. Such a model might simply include the effects of superheated dust or a fully self-consistent X-ray–heated atmosphere (e.g., Neufeld et al. 1994). Mid-IR photometry, or an IR spectrum, would motivate such a treatment, which might then better constrain the geometry of the inner disk.

REFERENCES

Abramowicz, M. A., Chen, X. M., Granath, M., & Lasota, J. P. 1996, ApJ, 471, 762
Abramowicz, M., Jaroszyński, M., & Sikora, M. 1978, A&A, 63, 221
Abramowicz, M., et al. 1995, ApJ, 438, L37
Bardeen, J. M., & Petterson, J. A. 1975, ApJ, 195, L65
Blandford, R. D. 1990, in Active Galactic Nuclei, Saas-Fee Advanced Course 20, ed. T. J.-L. Courvoisier & M. Mayor (Berlin: Springer)
———. 1998, Proc. Maryland Conference on Astrophysics, Some Like It Hot, ed. S. Holt & T. Kallman (New York: AIP), 43
Blandford, R. D., & Begelman, M. C. 1998, MNRAS, 303, L1
Blandford, R. D., & Znajek, R. L. 1977, MNRAS, 179, 433
Cao, X., & Jiang, D. R. 1997, A&A, 322, 49
Cecil, G., Morse, J. A., & Veilleux, S. 1995a, ApJ, 452, 613
Cecil, G., Wilson, A. S., & DePree, C. 1995b, ApJ, 440, 181
Cecil, G., Wilson, A. S., & Tully, R. B. 1992, ApJ, 390, 365
Chary, R., & Becklin, E. E. 1997, ApJ, 485, L75
Chen, X. M., Abramowicz, M. A., & Lasota, J.-P. 1997, ApJ, 476, 61
Chiang, E. I., & Goldreich, P. 1997, ApJ, 490, 368
Cizdziel, P. J., Wynn-Williams, C. G., & Becklin, E. E. 1985, AJ, 90, 731
Claussen, M. J., Heiligman, G. M., & Lo, K. Y. 1984, Nature, 310, 298
Claussen, M. J., & Lo, K. Y. 1986, ApJ, 308, 592
Gammie, C. F., & Popham, R. 1998, ApJ, 498, 313
Greenhill, L. J. et al. 1994, in Highlights of Astronomy, Vol. 10 (Dordrecht: Kluwer), 531
———. 1995a, ApJ, 440, 619
———. 1995b, A&A, 304, 21
Haardt, F., & Maraschi, L. 1991, ApJ, 380, 51
Haschick, A. D., & Baan, W. A. 1990, ApJ, 355, L23
Haschick, A. D., Baan, W. A., & Peng, E. W. 1994, ApJ, 356, 149
Herrnstein, J. R. 1997, Ph.D. thesis, Harvard Univ.
Herrnstein, J. R., Greenhill, L., & Moran, J. 1996, ApJ, 468, L17
Herrnstein, J. R., et al. 1998a, ApJ, 497, 69
———. 1998b, Nature, submitted
Herrnstein, J. R., et al. 1997a, ApJ, 475, L17
———. 1997b, BAAS, 191, 25.07
Ichimaru, S. 1977, ApJ, 214, 840
Konigl, A., & Kartje, J. F. 1994, ApJ, 434, 446
Kumar, P. 1997, ApJ, submitted (astro-ph/ 9706063)
Laor, A., & Draine, B. T. 1993, ApJ, 402, 441
Lasota, J. P., et al. 1996, ApJ, 462, 142
Mahadevan, R., & Quataert, E. 1997, ApJ, 490, 605
Makishima, K., et al. 1994, PASJ, 46, L77
Maoz, E., & McKee, C. F. 1997, ApJ, 494, 218
Martin, P., Roy, J.-R., Noreau, L., & Lo, K. Y. 1989, ApJ, 345, 707
Miyoshi, M., et al. 1995, Nature, 373, 127
Moran, J. M., et al. 1995, PNAS, 92, 11427
Nakai, N., Inoue, M., & Miyoshi, M. 1993, Nature, 361, 45
Nakamura, K. E., et al. 1997, PASJ, 49, 503
Narayan, R. 1997, in ASP Conf. Ser. 121, Proc. IAU Colloq. 163, Accretion Phenomena and Related Objects, ed. D. T. Wickramasinghe, L. Ferrario, & G. V. Bicknell (San Francisco: ASP), 75
Narayan, R., Kato, S., & Honma, F. 1997, ApJ, 476, 49
Narayan, R., Mahadevan, R., & Quataert, E. 1998a, The Theory of Black Hole Accretion Discs, ed. M. A. Abramowicz, G. Bjornsson, & J. E. Pringle (Cambridge: Cambridge Univ. Press), 148
Narayan, R., & Yi, I. 1994, ApJ, 428, 13
———. 1995a, ApJ, 444, 231
———. 1995b, Nature, 374, 623
Narayan, R., et al. 1998b, ApJ, 492, 554
Neufeld, D. A., & Maloney, P. R. 1995, ApJ, 447, L17 (NM)
Neufeld, D. A., Maloney, P. R., & Conger, S. 1994, ApJ, 436, L127
Papaloizou, J. C. B., & Pringle, J. E. 1983, MNRAS, 202, 1181
———. 1984, MNRAS, 208, 721
Phinney, E. S. 1989, in Theory of Accretion Disks, ed. W. Duschl et al. (Dordrecht: Kluwer), 457
Popham, R., & Gammie, C. F. 1998, ApJ, 504, 419
Pringle, J. E. 1981, ARA&A, 19, 137
———. 1996, MNRAS, 281, 357
Rees, M. J., Begelman, M. C., Blandford, R. D., & Phinney, E. S. 1982, Nature, 295 17
Rieke, G. H., & Lebofsky, M. J. 1978, ApJ, 220, L37
Rybicki, G. B., & Lightman, A. P. 1979, Radiative Processes in Astrophysics (New York: Wiley)
Sanders, D. B., et al. 1989, ApJ, 347, 29
Shakura, N. I., & Sunyaev, R. A. 1973, A&A, 24, 337
Shapiro, S. L., Lightman, A. P., & Eardley, D. M. 1976, ApJ, 204, 187
Spitzer, L. 1978, Physical Processes in the Interstellar Medium (New York: Wiley)
van Albada, G. D., & van der Hulst, J. M. 1982, A&A, 115, 263
Wallin, B. K., Watson, W. D., & Wyld, H. W. 1998, ApJ, 495, 774
Watson, W. D., & Wallin, B. K. 1994, ApJ, 432, L35
Wilkes, B. J., et al. 1995, ApJ, 455, L13